
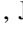






Radiogenic Heating and Its Influence on Rocky Planet Dynamos and Habitability

Francis Nimmo¹ , Joel Primack² , S. M. Faber³, Enrico Ramirez-Ruiz^{3,4} , and Mohammadtaher Safarzadeh³ 

¹Department of Earth and Planetary Sciences, University of California Santa Cruz, California, USA; fnimmo@ucsc.edu

²Physics Department, University of California Santa Cruz, 1156 High Street, Santa Cruz, CA 95064 USA

³Department of Astronomy, University of California Santa Cruz, 1156 High Street, Santa Cruz, CA 95064 USA

⁴Niels Bohr Institute, University of Copenhagen, Blegdamsvej 17, 2100 Copenhagen, Denmark

Received 2020 July 2; revised 2020 October 15; accepted 2020 October 17; published 2020 November 10

Abstract

The thermal evolution of rocky planets on geological timescales (Gyr) depends on the heat input from the long-lived radiogenic elements potassium, thorium, and uranium. Concentrations of the latter two in rocky planet mantles are likely to vary by up to an order of magnitude between different planetary systems because Th and U, like other heavy r -process elements, are produced by rare stellar processes. Here we discuss the effects of these variations on the thermal evolution of an Earth-size planet, using a 1D parameterized convection model. Assuming Th and U abundances consistent with geochemical models of the Bulk Silicate Earth based on chondritic meteorites, we find that Earth had just enough radiogenic heating to maintain a persistent dynamo. According to this model, Earth-like planets of stars with higher abundances of heavy r -process elements, indicated by the relative abundance of europium in their spectra, are likely to have lacked a dynamo for a significant fraction of their lifetimes, with potentially negative consequences for hosting a biosphere. Because the qualitative outcomes of our 1D model are strongly dependent on the treatment of viscosity, further investigations using fully 3D convection models are desirable.

Unified Astronomy Thesaurus concepts: [Extrasolar rocky planets \(511\)](#); [Earth \(planet\) \(439\)](#); [Super Earths \(1655\)](#); [Magnetic fields \(994\)](#); [Exoplanet evolution \(491\)](#); [R-process \(1324\)](#); [Stellar nucleosynthesis \(1616\)](#); [Astrobiology \(74\)](#)

1. Introduction

Rocky planets are gigantic heat engines (Stevenson 2008). They lose internal heat to the surface via some combination of conduction, convection, and advection, driving internal processes such as dynamo generation, volcanism, or plate tectonics as they do so. The internal heat arises in three ways: gravitational energy released as the planet formed; tidal heating, as for Io or some exoplanets (Henning & Hurford 2014); and decay of radioactive elements. Short-lived radionuclides such as ²⁶Al and ⁶⁰Fe may have contributed energy in the first ~ 3 Myr of our solar system and added to the primordial gravitational energy (reviewed in Lugaro et al. 2018). Long-lived radionuclides include ⁴⁰K, ²³²Th, ²³⁸U, and ²³⁵U and are the focus of this work. U and Th have been found in the Milky Way to be pure r -process products with concentrations that are characteristic of solar system matter but with sizable expected star-to-star bulk scatter in their concentrations with respect to lighter elements such as Mg (Snedden et al. 2008; Cowan et al. 2019). As a result, we expect other planetary systems to possess quite different concentrations of U and Th. Some geological consequences of such radiogenic element variations have been explored hitherto (Frank et al. 2014; Unterborn et al. 2015; Jellinek & Jackson 2015; Foley & Smye 2018; Botelho et al. 2019; Foley 2019; Quick et al. 2020; Wang et al. 2020). But to our knowledge the only paper examining how exoplanet dynamos would be affected by variations in U,Th is by O'Neill et al. (2020a), who assume these variations are small and correlate with core size. For reasons explained below we assume much larger, stochastic variations unconnected to core size.

For an Earth-mass body, the gravitational energy released by accretion is roughly 40 MJ kg^{-1} , whereas the total energy released by long-lived radioactive decay from formation to the

present is roughly 1 MJ kg^{-1} . But while accretion energy is delivered in short intervals during the first few Myr and thus sets the initial thermal conditions, radiogenic heating is an ongoing process occurring mostly in the mantle and crust. As a result, it is the latter that matters more for long-term geological evolution.

Estimates of radiogenic heat production for planets in our solar system rely heavily on the elemental concentrations found in primitive meteorites (see the Appendix). For the Earth, samples of the crust and upper mantle and direct measurements using geoneutrinos (Agostini et al. 2020) provide additional constraints. In the present day, plate tectonics causes the Earth to lose heat roughly twice as fast as it is being generated by radioactive decay (Sclater et al. 1980), so Earth is cooling. Four billion years ago, heat production was 3.5 times as large and the majority of heat transfer may have arisen through advection (volcanism; Moore & Webb 2013).

In the rocky planets, magnetic fields are generated by convection in a metallic core, which in turn is driven by heat extracted into the mantle (Nimmo 2015; Labrosse 2015; Boujibar et al. 2020). Since mantle radiogenic heat production controls how much heat is extracted from the core, it will also influence the presence or absence of a dynamo. Similarly, heat production will control the mantle temperature and thus the rate of silicate melting and volcanism.

Radiogenic heat production in the mantle is thus a key driver of rocky planet dynamics. Dynamics in turn affects planetary habitability (e.g., Lammer et al. 2009); for instance, atmospheric evolution depends on both volcanism and dynamo activity. As we argue below, rocky exoplanets may experience large variations in radiogenic heat production, from $\sim 30\%$ to $\sim 300\%$ of the terrestrial value. In this Letter we explore the

consequences of such variations for rocky planet dynamics and habitability.

2. Radiogenic Element Origins and Distribution

The elements that make up the rocky planets were formed by several nucleosynthetic pathways operating in precursor stars. Following dispersal into the interstellar medium and—ultimately—into a molecular cloud, when the cloud collapses to form a planetary system, these elements are incorporated mostly into the new star but also into smaller solid bodies of progressively increasing size. Such planetesimals may preferentially lose volatile elements (those with low condensation temperatures, such as potassium), as the solid-body assembly process typically involves periods of high temperature. Nonetheless, one would expect the planets’ final element concentrations to resemble those of the star they orbit, especially for refractory lithophile elements like Th and U. Thus, chemical abundance measurements of Galactic stars can be used to infer how the concentrations of various elements in their attendant planets are likely to vary, either spatially or in time.

From the point of view of long-term radiogenic heating, the most important elements are potassium, thorium, and uranium. Th and U are both *r*-process elements, most likely produced in neutron star mergers (NSMs; Kasen et al. 2017; Cowan et al. 2019), with possibly significant contributions also from massive star collapse explosions (Siegel et al. 2019; Macias & Ramirez-Ruiz 2019). Because such events are rare (an occurrence rate of \lesssim tens/Myr in our Galaxy) and produce large quantities of *r*-process elements, the resulting concentration of *r*-process elements should vary considerably. This is especially true of low-metallicity stars, because turbulent mixing of the interstellar medium is inefficient in the early Galaxy (Shen et al. 2015; Naiman et al. 2018). This expectation is in agreement with measurements of *r*-process europium in low-metallicity stars (e.g., Macias & Ramirez-Ruiz 2018) and with *r*-process abundances in dwarf galaxies (e.g., Ji et al. 2016).

Higher-metallicity stars also show larger variations of *r*-process elements than of elements (such as Mg) produced in core-collapse supernovae (e.g., Cowan et al. 2019). Measurements of short-lived *r*-process nuclide decay products (Hotokezaka et al. 2015) and relative concentrations (Bartos & Marka 2019) on Earth and in meteorites give further credence to the idea of a spatially inhomogeneous *r*-process distribution created by rare events such as NSMs.

The *r*-process element europium, which is easier to observe in stellar spectra than U or Th, is commonly used to measure the *r*-process content in stars and, as expected, appears to be a robust proxy for thorium (Botelho et al. 2019) and uranium (Sneden et al. 2008), despite complications arising from decay of ^{235}U and severe blending of the Th II line. The quantity $[\text{Eu}/\text{H}]$ shows a range of -0.5 to $+0.5$ for Milky Way disk stars and shows a roughly linear correlation with $[\text{Fe}/\text{H}]$ (Battistini & Bensby 2016). For thermal evolution models, what matters is the rate of heat production per unit mass of silicates. As a result, the most relevant metric is the concentration of Eu (a proxy for U and Th) compared with that of the alpha elements Mg and Si (proxies for the bulk silicate mantle). The 10%–90% percentile range observed in $[\text{Eu}/\text{Mg}]$ is from about -0.3 to $+0.3$ for likely planet-hosting stars (i.e., those with $[\text{Mg}/\text{H}] > -0.3$; Battistini & Bensby 2016; Delgado Mena et al. 2017, 2019; Griffith et al.

2019), while based on the Hypatia catalog (<https://www.hypatiacatalog.com/>), the 1%–99% range is about -0.5 to $+0.5$, or 30% to 300% (Hinkel et al. 2014). The Eu/Mg ratio is likely to be a good indicator of the variation in volumetric heat production between planets orbiting different stars in the disk because of the expected correspondence between host star and planet compositions.

In contrast to Th and U, potassium is produced in SNe II (^{39}K ; Shimansky et al. 2003) and via *s*-process nucleosynthesis (^{40}K ; The et al. 2007). Because neither pathway is rare, spatial variations in potassium between stars are expected to be limited (Lugaro et al. 2018). However, rocky bodies in our solar system exhibit large variations in K concentrations (McCubbin et al. 2012) because K is much more volatile, and thus more susceptible to loss during accretion, than U or Th. Alpha elements such as Mg and Si, which make up rocky planet mantles are neither volatile nor expected to show as much variability as *r*-process elements (Sneden et al. 2008). Stellar Mg/Si ratios show only tens of percent variability (Brewer & Fischer 2018), in agreement with measurements from polluted white dwarfs, which provide estimates of planet composition (Doyle et al. 2019). In summary, we expect Th and U to exhibit variations in concentration relative to Mg from 30 to 300% of the solar system value between different Sun-like stars in our Galaxy (and their associated planets). While K might exhibit volatile-related variability between (or within) stellar systems, such variations are much harder to predict a priori, and the overall contribution of ^{40}K to the present-day heat budget is in any case quite modest. Below we focus on the effect on radiogenic heating of rocky planets with a wide range of Th and U concentrations.

The Earth’s total present-day surface heat flow is in the range 42–47 TW (Sclater et al. 1980; Davies & Davies 2010), or 35–40 TW when the radiogenic contribution of the crust is subtracted (Sclater et al. 1980; O’Neill et al. 2020b). The total radiogenic heat production of the Earth is about 22 TW, based on chondritic meteorites (reviewed in O’Neill et al. 2020b), of which about 15 TW is sourced within the mantle. These are similar to what we assume for our fiducial Earth model discussed below. However, we note that geoneutrinos from the ^{238}U and ^{232}Th decay chains detected by Borexino have recently led to a much higher estimate of the Earth’s total radiogenic heat of $38.2^{+13.6}_{-12.7}$ TW, and a total mantle heat contribution of $24.6^{+11.1}_{-10.4}$ TW (Agostini et al. 2020).

3. Thermal Evolution

Below we carry out some simple explorations of how the initial radiogenic element concentration affects rocky planet evolution. We focus on Earth-mass planets with the same terrestrial mineralogy and use a parameterized convection approach modified from Nimmo et al. (2004), in which plate-tectonic-like heat transfer is assumed. Because planetary dynamos are more likely to arise when plate tectonics is operating (Nimmo 2002), we do not address the contentious issue of whether plate tectonic or stagnant lid convection is more likely on exo-Earths (e.g., Tackley et al. 2013; Noack & Breuer 2014; Weller & Lenardic 2016).

Fully 3D, and even 2D, fluid dynamical models of Earth’s thermal evolution are computationally expensive. As a result, parameterized convection models, which provide an averaged 1D description of mantle evolution, are frequently used, and are found to provide a reasonable match to 2D or 3D models (e.g.,

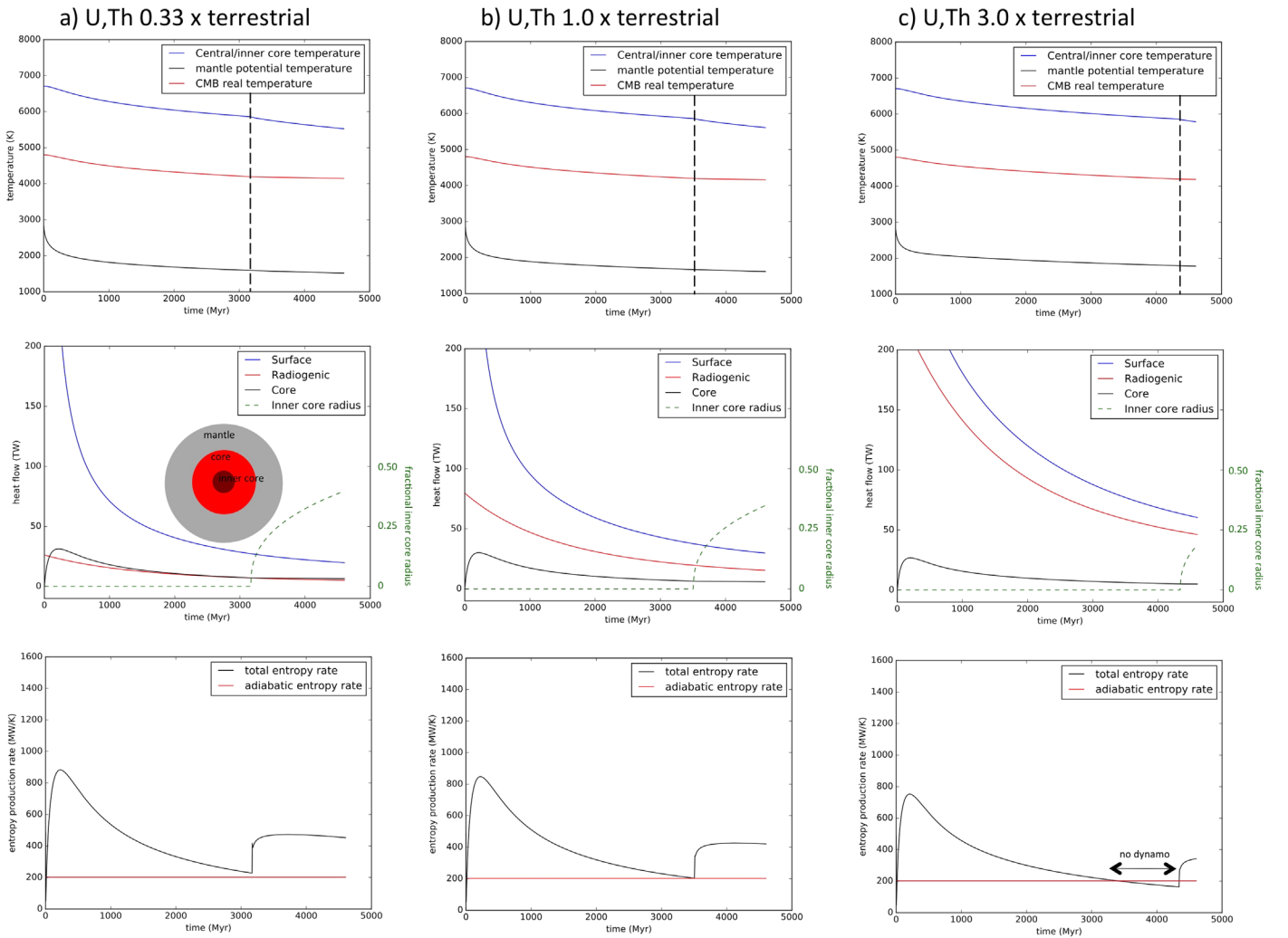


Figure 1. Effect on thermal evolution and dynamo for different concentrations of radiogenic elements (U,Th): a) 33% of terrestrial; b) 100% of terrestrial; c) 300% of terrestrial. In each column the top plot shows temperature evolution, the middle plot shows heat flow and solid inner core radius, and the bottom plot the net rate of entropy production (driving a dynamo requires a value greater than the adiabat). Present-day is at the end of the plots. The inset in column a) shows the internal structure of the Earth. Vertical lines in top panels denote onset of inner core solidification.

Van Keken 2001; Thiriet et al. 2019), though they cannot capture the full complexity of a numerical model. In the parameterized approach of Nimmo et al. (2004), heat fluxes at both the top and bottom of the mantle are calculated by assuming that the local (boundary layer) Rayleigh number is at the critical value for convection. Based on the suggestion of Davies (2007) we modified the original bottom heat flux calculation (see the Appendix); this produces qualitatively different results to the unmodified approach. Our modified model yields results that are qualitatively consistent with the numerical convection models of Plesa et al. (2015) for Mars, but should be regarded as somewhat provisional until they are checked by future numerical experiments.

Mantle viscosity is temperature-dependent and is set to a reference value at a reference temperature; the reference viscosity at the bottom is higher than that at the top to mimic the effects of increased pressure and phase transitions. The initial temperatures of the core and mantle are set to be the same at the core-mantle boundary (CMB). The temperature gradient in the mantle is assumed to be adiabatic, because individual convecting parcels do not have time to exchange heat with their surroundings.

The Earth’s dynamo arises from fluid motions in its iron core. These fluid motions are acted on by the Earth’s rotation, but are ultimately driven by some combination of thermal and compositional buoyancy. The thermal buoyancy occurs because of extraction of heat from the core into the mantle; compositional buoyancy occurs as the solid inner core grows and releases light elements (e.g., Si or O) into the fluid above. Solid inner core growth starts only when the core has cooled sufficiently, so that for much (~60%–90%) of Earth history a solid inner core was absent. As reviewed by Nimmo (2015) and Labrosse (2015), maintaining a well-mixed, convecting core in the absence of compositional buoyancy requires that the heat extracted from the core must exceed the adiabatic value. A more general approach (which includes the effect of composition) is to track the rate of entropy production rather than heat extraction (e.g., Nimmo et al. 2004). Tracking the net entropy production rate $\Delta\dot{E}$ thus provides a simple proxy for whether a dynamo can operate or not, while the dipole field strength is expected to scale as $\Delta\dot{E}$ to one-third power (Labrosse 2015).

Figure 1(b) (middle column) illustrates our baseline result, with parameters chosen so that the present-day known characteristics of the Earth (mantle temperature and viscosity

structure, heat flux budget, inner core radius) and petrological constraints on mantle temperature evolution (Abbott et al. 1994) are reproduced. Although this particular set of parameter choices (notably the thermal conductivity of the core) is non-unique, the main point of this exercise is to isolate the effect of changing one particular parameter (radiogenic heat production) and to examine its consequences.

The top panel shows the decline in core and mantle temperatures as a function of time, with the present-day mantle temperature projected to the surface (the potential temperature) T_p of 1341 °C and cooling rate of 50 K/Gyr in approximate agreement with petrological constraints (Abbott et al. 1994). The middle panel shows heat flow evolution, with a present-day mantle radiogenic heat production rate of 15 TW and surface and core heat flows of 30 and 6 TW, respectively. It also shows the growth of the inner core, which starts to solidify at 3515 Myr (1.05 Ga) as the core cools. The bottom panel shows that the resulting rate of entropy production exceeds the adiabatic value and is thus sufficient to maintain a dynamo, except possibly for a brief period just prior to inner core formation. The entropy production rate increases markedly once the inner core starts to grow, because compositional buoyancy is now aiding thermal buoyancy. Paleomagnetic measurements show that a terrestrial dynamo has operated over at least the last 3.5 Gyr (Tarduno et al. 2010), with at least one interval lasting up to a few Myr of low- or no-field (Bono et al. 2019).

Because of the energetic nature of Earth accretion, the appropriate initial conditions are highly uncertain. Fortunately, they turn out not to be very important: because mantle heat transport is highly dependent on temperature, mantle temperature evolution is controlled mainly by radiogenic heat production. Thus, increasing the start temperature by 500 K changes the present-day potential temperature by less than 1.5 K; Schubert et al. (1980) found an almost identical result. Starting with a core hotter than the mantle likewise has little effect at the present day.

Figures 1(a) and (c) show how an identical model evolves with the same initial conditions except for 0.33 and 3 times the assumed terrestrial concentrations of U and Th. Less and more radiogenic heating result in colder and warmer present-day mantles (ΔT_p) of -99 K and $+166$ K, respectively; these results resemble those of Unterborn et al. (2015). The behavior of the core is more complicated, because of the competing effects of changes in the core-mantle temperature contrast and mantle viscosity (see the Appendix). The former effect alone would decrease the core heat flux in a hotter mantle, while the latter would increase it. Somewhat counter-intuitively, we find that more mantle heating results in a lower present-day core heat flux, a smaller inner core and a less vigorous dynamo, and vice versa. The case with enhanced mantle heating (Figure 1(c)) experiences a dynamo that ceases to operate for hundreds of Myr.

Figure 2 shows the net rate of entropy production (colors: a proxy for dynamo strength) as a function of time and radiogenic element fraction. The three trajectories shown in Figure 1 are marked as horizontal dashed lines, and the contour lines denote the mantle potential temperature. As noted above, higher radiogenic element concentrations result in hotter mantles, smaller present-day inner cores and longer periods in which a dynamo is absent.

4. Summary

Our simplified model shows that higher concentrations of U, Th have two principal consequences: one is hotter present-day mantles; the other is reduced dynamo activity. The converse is true for lower U,Th concentrations. Both of these effects are likely to have major implications for habitability.

A global magnetic field modifies the trajectories of charged particles emitted by the host star. In our solar system the net effect of such a field is probably to reduce rates of long-term atmospheric loss due to particle bombardment (Lundin et al. 2007) though this is debated (Gunell et al. 2018). How such effects would translate to close-in Earth-like exoplanets is uncertain (Owen 2019) but, overall, dynamo activity is regarded as an important component of planetary habitability (Lammer et al. 2009).

Assuming a similar bulk mantle composition (in terms of major elements: Mg, Si etc.), higher mantle temperatures will yield more melting (and thus volcanic activity) and higher convective velocities, both of which will produce higher melt generation rates. Because volatile elements (like water) tend to concentrate in silicate melts, higher total melt production will result in more efficient outgassing from the interior. The likely consequence is a more volatile-rich surface and/or a thicker atmosphere, depending on the degree of volatile return to the interior by plate tectonics (e.g., Noack & Breuer 2014; Foley & Smye 2018).

Early discussions of planetary habitability focused on the orbital semimajor axis and stellar flux (Hart 1979). More recent investigations have added other factors of interest (e.g., Lammer et al. 2009), including the abundance of *r*-process elements (e.g., Frank et al. 2014), which we argue here will help determine both dynamo and volcanic outgassing activity. An important aspect of this particular factor is that *it can be determined by observations*. As discussed above, planetary concentrations of U and Th are expected to track those of the host star, which can be measured via spectroscopy through the surrogate element Eu (e.g., Botelho et al. 2019; Lin et al. 2020). For instance, da Silva et al. (2016) showed an increase in Eu (and by inference Th and U) relative to Fe of roughly 0.5 dex from the Galactic center to the outer disk. We conclude that stellar abundances of K, Th, and U should be taken into account in designing future observational campaigns.

5. Discussion/Future Work

The calculations shown in Figures 1 and 2 are highly simplified. In particular, although they are tuned to match existing constraints on Earth’s present-day state and evolution, they become progressively more uncertain at earlier times, when the initial conditions chosen are more important and unmodeled processes (e.g., melt advection, different tectonic styles) may operate. Furthermore, as noted above, even the qualitative behavior of the core heat flux is sensitive to particular modeling choices (see the Appendix). 2D or 3D convection models investigating the role of radiogenic heat production on exoplanet heat transfer—along the lines of O’Neill et al. (2020a)—can capture details (e.g., the effect of phase transitions) not treated here, and resolve current uncertainties in the link between radiogenic heating and core heat flux.

The models shown in Figure 1 all assume plate-tectonic like heat transfer. But the example of Venus shows that even for

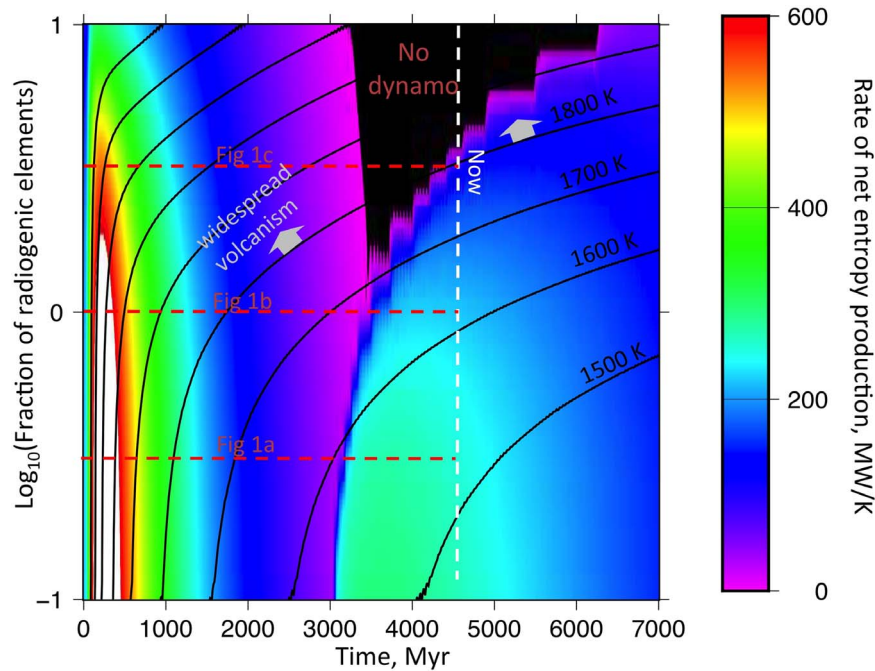


Figure 2. Sensitivity of evolution of core parameters to different radiogenic element concentrations (relative to the nominal terrestrial case). The colors show the rate of net entropy production, with black indicating a negative value (no dynamo). The contours denote the mantle potential temperature. The three dashed red lines show the trajectories of the three evolution scenarios shown in Figure 1. The vertical white dashed line indicates present day.

Earth-like planets, plate tectonics is not assured. Because plate tectonics cools the mantle (and thus the core) efficiently, long-term plate tectonics is likely crucial to the maintenance of a dynamo (Nimmo 2002). Unfortunately, exactly what determines whether plate tectonics occurs is not understood; the presence of water (and thus the eccentricity and semimajor axis of the planet’s orbit) and/or melt are likely important (Lourenço et al. 2018), and so too are the mantle driving stresses, and thus the heat production rate (O’Neill et al. 2020a). Since the survival of water and the generation of melt are in turn both sensitive to the radiogenic abundance, predicting how these factors interact with each other is not straightforward.

How would planetary radius influence our conclusions? A larger planet produces more radiogenic heat per unit area; to first order the heat fluxes will therefore scale with radius R . But the minimum (adiabatic) heat flux required to drive a dynamo also scales with gravity, and thus also with R . So larger planets are not guaranteed to have more vigorous dynamos (though we do expect them to be more volcanically active); more detailed treatments are required, such as those of Boujibar et al. (2020) but including radiogenic heating.

Spatial and temporal variability in radiogenic element concentrations will also play a role. As noted above, U and Th concentrations are expected to increase toward the edge of the Galactic disk (da Silva et al. 2016). The age of the planet is more complicated. Obviously, other things being equal an older planet will have lower radiogenic heat production (because the nuclides will have decayed) and a weaker or absent dynamo. Furthermore, Delgado Mena et al. (2019) showed that the stellar Eu/Mg ratio decreases with increasing stellar age at about 0.1 dex per 10 Gyr, compounding this effect. In O’Neill et al. (2020a) the stellar age is assumed to cause the core size (via the ratio Mg/Fe) and radiogenic heat production to covary. By contrast, in our view the impact of any secular

variation in initial U,Th concentrations will be less important than the expected random scatter. In any event, more general explorations of the role of r -process elements in determining planetary behavior, and the specific influence of core size, planet size, and plate tectonics on habitability, are of interest to pursue in future.

Our results are summarized in Figure 2: higher mantle heating rates increase volcanic activity and shut off the dynamo, both likely deleterious for habitability. In contrast, reduced mantle heating rates will at some point stop melt production. A potential consequence is that plate tectonics will then cease (Lourenço et al. 2018), and with it, the dynamo, as at Venus (Nimmo 2002). It is tempting to speculate that the Earth is habitable in part because it possesses a “Goldilocks” concentration of radiogenic elements: high enough to permit long-lived dynamo activity and plate tectonics, but not so much that extreme volcanism and dynamo shutoff occur. As yet, however, our understanding of the complicated feedbacks involved is too rudimentary to make such a definitive conclusion; more detailed calculations, and better characterization of the radiogenic element abundances in planet-hosting stars, are both required.

E.R.-R. thanks the Heising-Simons Foundation, and the Danish National Research Foundation (DNRF132) for support. S.M.F. acknowledges support from NSF AST-1615730. We thank Natalie Batalha, Ben Zuckerman, Matt Shetrone, David Weinberg, Ina Plesa, Steve Ritz, and Charli Sakari for helpful discussions, and the reviewer for insightful comments.

Appendix

Below we provide some additional details on the implementation of the parameterized convection; parameter values not discussed here are the same as in Nimmo et al. (2004). We

also note here that in our analysis of the Hypatia catalog (Hinkel et al. 2014) we exclude the data of Luck (2015, 2017, 2018) from our results, since these show anomalously high Eu concentrations. Thus, the range for [Eu/Mg] of -0.5 to $+0.5$ dex is conservative and would be higher if the Luck data were included.

Following O'Neill et al. (2020b) we assume initial Bulk Silicate Earth concentrations of 260 ppm, 23 ppb and 85 ppb, respectively, for K, U and Th; this produces 22 TW of heat production at the present day. We implicitly assume that the major element chemistry and mineralogy is the same as that of Earth; these variables are expressed in the model via the reference viscosities and activation energy assumed for the mantle. We assume that the convecting mantle is responsible for 70% of the total radiogenic heat at all times; the remainder is assumed to reside in the crust and will not contribute to mantle thermal evolution. In examining the effect of varying radiogenic element concentrations, we allow U and Th concentrations to vary from their nominal value but keep the K concentration the same, because only r -process elements are expected to show large variations from star to star (see the main text).

As discussed in more detail below, heat transfer across the top and bottom boundary layers of the mantle is calculated by using a local Rayleigh number approach. The heat flux out of the core is affected by two competing processes. A hotter mantle has a lower viscosity, and thus a tendency to increase the heat flux; but it also decreases the core-mantle temperature difference, lowering the heat flux. Because of these competing effects, we find that small changes in model assumptions can lead to qualitatively different behavior. We adopt an approach suggested by Davies (2007; see below), but note that future numerical models are required to check this approach.

The bottom boundary layer thickness δ_b is given by

$$\delta_b = \left[\frac{Ra_c \kappa_b \eta_b}{\rho_m g \alpha_m (T_c - T_m)} \right]^{1/3}$$

where Ra_c is the critical Rayleigh number (set to 600), κ_b , ρ_m , and α_m are the mantle thermal diffusivity, density, and thermal expansivity, g is the acceleration due to gravity and T_c and T_m are the core temperature at the CMB and the mantle temperature projected down to the CMB along the adiabat, respectively.

The viscosity η_b was evaluated by Nimmo et al. (2004) at the mean boundary layer temperature ($T_a = [T_c + T_m]/2$). But it was argued in Davies (2007) that for a bottom boundary layer it is more appropriate to evaluate the viscosity at T_c instead, and we follow this approach here.

The basal viscosity at a temperature T is evaluated according to

$$\eta_b(T) = f\eta_0 \exp[-\xi(T - T_0)]$$

where η_0 is the reference viscosity at a reference temperature T_0 , f is a factor used to account for the intrinsically higher viscosity of the lower mantle, and ξ describes the temperature sensitivity of the viscosity and is taken to be 0.01 K^{-1} here. At the nominal present-day reference viscosity and mantle temperature of $1341 \text{ }^\circ\text{C}$ the upper- and lower-mantle viscosities are 1.3×10^{21} and 1.6×10^{22} Pa s.

The CMB heat flux is then given by $F_b = k_b (T_c - T_m)/\delta_b$ where k_b is the thermal conductivity at the base of the mantle.

Because of the sensitivity of the core heat flux to two opposing effects (see above), heat flux results using $\eta_b(T_a)$ yield quite different results to those using $\eta_b(T_c)$. Uncertainties in what reference viscosity η_0 to assume, while large, are less important than deciding whether to use $\eta_b(T_c)$ or $\eta_b(T_a)$ because we can determine the reference viscosity by needing to reproduce the present-day Earth characteristics.

We adopt the $\eta_b(T_c)$ approach advocated by Davies (2007) because it produces results that are qualitatively consistent with the numerical models of Plesa et al. (2015). Specifically, these authors find that higher mantle heat production rates yield higher mantle and core temperatures and (in general) lower time-averaged core heat fluxes, which agrees with our findings. Furthermore, our heat flux results are in line with the numerical models of O'Neill et al. (2020a), though the latter may still be experiencing initial transients.

The surface heat flux is calculated using similar expressions except that: the driving temperature difference is $T'_m - T_s$ where T'_m and T_s are the mantle potential temperature and surface temperature; and the thermal diffusivity and thermal conductivity are assumed lower than in the lower mantle.


The core thermal conductivity is here taken to be $50 \text{ W m}^{-1} \text{ K}^{-1}$ and 100 ppm potassium is assumed to be present in the core. Parameter values different from the nominal values used in Nimmo et al. (2004) are as follows: mantle bulk density $\rho_m = 4400 \text{ kg m}^{-3}$, reference viscosity $\eta_0 = 2 \times 10^{21}$ Pa s, lower-mantle viscosity factor $f = 20$, and the reference temperature for the lower mantle is $T_0 = 4070 \text{ K}$.

ORCID iDs

Francis Nimmo  <https://orcid.org/0000-0003-3573-5915>

Joel Primack  <https://orcid.org/0000-0001-5091-5098>

Enrico Ramirez-Ruiz  <https://orcid.org/0000-0003-2558-3102>

Mohammadtaher Safarzadeh  <https://orcid.org/0000-0002-1827-7011>

References

- Abbott, D., Burgess, L., Longhi, J., & Smith, W. H. F. 1994, *JGR*, **99**, 13835
- Agostini, M., Altenmüller, K., Appel, S., et al. 2020, *PhRvD*, **101**, 012009
- Bartos, I., & Marka, S. 2019, *Natur*, **569**, 85
- Battistini, C., & Bensby, T. 2016, *A&A*, **586**, A49
- Bono, R. K., Tarduno, J. A., Nimmo, F., & Cottrell, R. D. 2019, *NatGe*, **12**, 143
- Botelho, R. B., Milone, A. d. C., Meléndez, J., et al. 2019, *MNRAS*, **482**, 1690
- Boujibar, A., Driscoll, P., & Fei, Y. 2020, *JGRE*, **125**, e06124
- Brewer, J. M., & Fischer, D. A. 2018, *ApJS*, **237**, 38
- Cowan, J. J., Sneden, C., Lawler, J. E., et al. 2019, arXiv:1901.01410
- da Silva, R., Lemasle, B., Bono, G., et al. 2016, *A&A*, **586**, A125
- Davies, G. F. 2007, *PEPI*, **160**, 215
- Davies, J. H., & Davies, D. R. 2010, *SoLE*, **1**, 5
- Delgado Mena, E., Tsantaki, M., Adibekyan, V. Z., et al. 2017, *A&A*, **606**, A94
- Delgado Mena, E., Moya, A., Adibekyan, V., et al. 2019, *A&A*, **624**, A78
- Doyle, A. E., Young, E. D., Klein, B., Zuckerman, B., & Schlichting, H. E. 2019, *Sci*, **366**, 356
- Foley, B. J. 2019, *ApJ*, **875**, 72
- Foley, B. J., & Smye, A. J. 2018, *AsBio*, **18**, 873
- Frank, E. A., Meyer, B. S., & Mojzsis, S. J. 2014, *Icar*, **243**, 274
- Griffith, E., Johnson, J. A., & Weinberg, D. H. 2019, *ApJ*, **886**, 84
- Gunell, H., Maggiolo, R., Nilsson, H., et al. 2018, *A&A*, **614**, L3
- Hart, M. H. 1979, *Icar*, **37**, 351
- Henning, W. G., & Hurford, T. 2014, *ApJ*, **789**, 30
- Hinkel, N. R., Timmes, F. X., Young, P. A., Pagano, M. D., & Turnbull, M. C. 2014, *AJ*, **148**, 54
- Hotokezaka, K., Piran, T., & Paul, M. 2015, *NatPh*, **11**, 1042

- Jellinek, A. M., & Jackson, M. G. 2015, *NatGe*, 8, 587
- Ji, A. P., Frebel, A., Chiti, A., & Simon, J. D. 2016, *Natur*, 531, 610
- Kasen, D., Metzger, B., Barnes, J., Quataert, E., & Ramirez-Ruiz, E. 2017, *Natur*, 551, 80
- Labrosse, S. 2015, *PEPI*, 247, 36
- Lammer, H., Bredehöft, J. H., Coustenis, A., et al. 2009, *A&ARv*, 17, 181
- Lin, J., Asplund, M., Ting, Y.-S., et al. 2020, *MNRAS*, 491, 2043
- Lourenço, D. L., Rozel, A. B., Gerya, T., & Tackley, P. J. 2018, *NatGe*, 11, 322
- Luck, R. E. 2015, *AJ*, 150, 88
- Luck, R. E. 2017, *AJ*, 153, 21
- Luck, R. E. 2018, *AJ*, 155, 111
- Lugaro, M., Ott, U., & Kereszturi, Á 2018, *PrPNP*, 102, 1
- Lundin, R., Lammer, H., & Ribas, I. 2007, *SSRv*, 129, 245
- Macias, P., & Ramirez-Ruiz, E. 2018, *ApJ*, 860, 89
- Macias, P., & Ramirez-Ruiz, E. 2019, *ApJL*, 877, L24
- McCubbin, F. M., Riner, M. A., Vander Kaaden, K. E., & Burkemper, L. K. 2012, *GeoRL*, 39, L09202
- Moore, W. B., & Webb, A. A. G. 2013, *Natur*, 501, 501
- Naiman, J. P., Pillepich, A., Springel, V., et al. 2018, *MNRAS*, 477, 1206
- Nimmo, F. 2002, *Geo*, 30, 987
- Nimmo, F. 2015, in *Treatise on Geophysics*, Vol. 9 ed. G. Schubert (Amsterdam: Elsevier), 201
- Nimmo, F., Price, G. D., Brodholt, J., & Gubbins, D. 2004, *GeoJI*, 156, 363
- Noack, L., & Breuer, D. 2014, *P&SS*, 98, 41
- O'Neill, C., Lowman, J., & Wasiliev, J. 2020a, *Icar*, 352, 114025
- O'Neill, C., O'Neill, H. S. C., & Jellinek, A. M. 2020b, *SSRv*, 216, 37
- Owen, J. E. 2019, *AREPS*, 47, 67
- Plesa, A. C., Tosi, N., Grott, M., & Breuer, D. 2015, *JGRE*, 120, 995
- Quick, L. C., Roberge, A., Mlinar, A. B., & Hedman, M. M. 2020, *PASP*, 132, 084402
- Schubert, G., Stevenson, D. J., & Cassen, P. 1980, *JGR*, 85, 2531
- Sclater, J. G., Jaupart, C., & Galson, D. 1980, *RvGSP*, 18, 269
- Shen, S., Cooke, R. J., Ramirez-Ruiz, E., et al. 2015, *ApJ*, 807, 115
- Shimansky, V. V., Bikmaev, I. F., Galeev, A. I., et al. 2003, *ARep*, 47, 750
- Siegel, D. M., Barnes, J., & Metzger, B. D. 2019, *Natur*, 569, 241
- Snedden, C., Cowan, J. J., & Gallino, R. 2008, *ARA&A*, 46, 241
- Stevenson, D. J. 2008, *Natur*, 451, 261
- Tackley, P. J., Ammann, M., Brodholt, J. P., Dobson, D. P., & Valencia, D. 2013, *Icar*, 225, 50
- Tarduno, J. A., Cottrell, R. D., Watkeys, M. K., et al. 2010, *Sci*, 327, 1238
- The, L.-S., El Eid, M. F., & Meyer, B. S. 2007, *ApJ*, 655, 1058
- Thiriet, M., Breuer, D., Michaut, C., & Plesa, A.-C. 2019, *PEPI*, 286, 138
- Unterborn, C. T., Johnson, J. A., & Panero, W. R. 2015, *ApJ*, 806, 139
- Van Keken, P. 2001, *PEPI*, 124, 119
- Wang, H. S., Morel, T., Quanz, S. P., & Mojzsis, S. J. 2020, *A&A*, in press (doi:10.1051/0004-6361/202038386)
- Weller, M. B., & Lenardic, A. 2016, *GeoRL*, 43, 9469